Numerical Simulation of Anisotropic Surface Diffusion with Curvature-dependent Energy

Martin Burger *
Department of Mathematics, UCLA,
520 Portola Plaza, Los Angeles, CA 90095, USA.

February 12, 2004

Abstract

The aim of this paper is the numerical simulation of surface diffusion processes in the presence of a strong anisotropy and curvature dependence in the surface energy. We derive semi-implicit finite element discretizations based on a splitting into three second-order equations. The discretization we use yields indefinite linear systems for the nodal values of the height function, the curvature concentration, and the chemical potential.

We provide several numerical examples and parametric studies with respect to some of the parameters in the surface energy and with respect to the coverage. The results, to our knowlegde the first that have been obtained for this model, confirm theoretical predictions, namely partial faceting of the surfaces with rounded corners.

Keywords: Surface Diffusion, Crystal Growth, Faceting, Finite Element Method

AMS Subject Classification: 65M60, 74N20, 74N25, 74E10, 35K30, 35K55

PACS: 02.60.Lj, 81.10.Aj, 64.70.Nd, 68.03.Cd

1 Introduction

Anisotropic surface diffusion processes (cf. [6, 9, 21]) are of high importance in modern material and nano science. The applications range from the self-organized growth of nanostructures over crystal growth, shape transitions in

*On leave from: Industrial Mathematics Institute, Johannes Kepler Universität Linz. e-mail: martin.burger@jku.at.

alloys, to the formation of basalt columns caused by volcanic activities. Of particular importance are systems with a strongly anisotropic non-convex surface energy. In this case, the surface diffusion flow may lead to *faceted surfaces*, i.e., surfaces composed by plane segments whose orientation is determined by the specific anisotropic surface tension. Using this representation, simulations of strongly anisotropic diffusion processes based on the solution of ordinary differential equations have been carried out in [7, 25].

However, many observed interfaces are not fully faceted, but rather have rounded corners. As a model for this effect, it has been proposed by several authors (cf. [14, 15, 16, 17, 23, 24]) to incorporate a higher-order term dependent on the mean curvature of the surface into the surface energy functional. The corresponding flow is a sixth-order parabolic partial differential equation with strong nonlinearities, which is difficult to solve numerically. Previous simulations were based on asymptotic models obtained from long-wave expansions (cf. [14, 15, 23]), but to our knowledge no simulations have been performed for the exact model yet. The aim of this paper is the development of numerical methods for the full model of anisotropic surface diffusion processes with curvature-dependent energy.

Our approach is based on a splitting into three second-order equations, which is motivated by the recently proposed methods for isotropic and weakly anisotropic surface diffusion (cf. [1, 2, 11]) using a splitting of fourth-order flows into two equations. In the case of the flow of a curve in $\mathbb{R}^2$ (which one might also call *curve diffusion* for obvious reasons), the splitting can be performed in a rather straight-forward way using the chemical potential and the mean curvature as additional variables, while the situation is more complicated for a surface in $\mathbb{R}^3$. We shall demonstrate below that a "curvature concentration" should be used instead of the curvature and the time discretization should be based on a local-in-time variational principle. Due to the differences between curve and surface diffusion we shall treat their numerical simulation in different sections of this paper.

For simplicity and since it is a very realistic assumptions for many practical applications we shall always assume that the interface (surface or curve) can be represented as the graph of a function. We denote the evolving interface by Γ and represent it as the graph of a function u over a fixed domain $\Omega \subset \mathbb{R}^d$, $d = 1, 2$, i.e.,

$$\Gamma(t) = \{\ (\mathbf{x}, u(\mathbf{x}, t)) \mid \mathbf{x} \in \Omega\ \}. \tag{1.1}$$

Corresponding to this representation, the normal $\mathbf{n}$, the length of a surface

element Q, and the mean curvature κ are given by

$$Q = \sqrt{1 + |\nabla u|^2}, \qquad \mathbf{n} = \frac{1}{Q}(-\nabla u, 1), \qquad \kappa = \operatorname{div}\left(\frac{\nabla u}{Q}\right). \tag{1.2}$$

Following [16, 17] we assume the surface energy to be of the form

$$\mathcal{E}(u) = \int_\Omega \gamma(\mathbf{n}, \kappa)\ Q\ d\mathbf{x}, \tag{1.3}$$

with the surface tension

$$\gamma(\mathbf{n}, \kappa) = \alpha(1 + \epsilon \sum_{j=1}^{d+1} n_j^4 + \nu\kappa^2), \tag{1.4}$$

for positive parameters α, ϵ, and ν. We want to mention that our approach is able to deal with more general surface energies of the form

$$\gamma(\mathbf{n}, \kappa) = \alpha(1 + \gamma_0(\mathbf{n}) + \nu\kappa^2),$$

with only minor modifications.

The surface diffusion flow corresponding to this surface energy and including deposition effects is obtained via the velocity

$$\mathbf{V} = \mathbf{F} - \frac{D_S\Omega^2\sigma}{kT}(\Delta_S\mu)\ \mathbf{n} \qquad \text{on } \Gamma, \tag{1.5}$$

where $\mathbf{F}$ is a deposition flux, D_S a diffusion coefficient of the adatoms, Ω the atomic volume, σ the surface density, k the Boltzmann constant, and T the temperature. The variable μ denotes the *chemical potential* given as the negative variation of the surface energy with respect to the surface, i.e., with the above graph representation

$$\mu = -\mathcal{E}'(u). \tag{1.6}$$

By taking the inner product of the velocity $\mathbf{V}$ and the normal $\mathbf{n}$, we obtain a partial differential equation for the height function u as

$$\frac{\partial u}{\partial t} = -\frac{D_S\Omega^2\sigma}{kT}\ \operatorname{div}\left(\frac{\nabla\mu}{Q}\right) + \mathbf{F}\cdot(-\nabla u, 1). \tag{1.7}$$

For the sake of simplicity we shall assume in the following that the scaling of time and chemical potential are such that $\alpha = 1$ and $\frac{D_S\Omega^2\sigma}{kT} = 1$. Moreover, we consider the simple, but realistic case of a deposition in vertical

direction, i.e., $\mathbf{F} = f\mathbf{e}_z$ and thus, $\mathbf{F} \cdot (-\nabla u, 1) = f$. Hence, the partial differential equation for u we shall investigate is given by

$$\frac{\partial u}{\partial t} = -\operatorname{div}\left(\frac{\nabla \mu}{Q}\right) + f. \tag{1.8}$$

The relation (1.8) looks like a low order partial differential equation at the first glance, but a detailed investigation of (1.6) for the above form of the surface energy will show that $\mathcal{E}'(u)$ correponds to a fourth-order differential operator applied to u, and hence, (1.8) is a sixth-order equation. The boundary conditions we shall use are homogeneous Neumann conditions, i.e.,

$$\nabla u \cdot \mathbf{n}_{\partial\Omega} = \nabla(Q\kappa) \cdot \mathbf{n}_{\partial\Omega} = \nabla \mu \cdot \mathbf{n}_{\partial\Omega} = 0, \qquad \text{on } \partial\Omega, \tag{1.9}$$

where κ denotes the mean curvature and μ the chemical potential (see the next section for detailed definitions). An alternative model used in several cases are periodic boundary conditions, which could easily be incorporated into our approach.

This paper is organized as follows: In Section 2 we discuss the basic properties of anisotropic surface diffusion such as volume conservation, energy decay, and the variations of the surface energy. Using a variational principle for the surface diffusion flow, we derive a semi-implicit finite element method in Section 3, and discuss the solution of the arising finite-dimensional problems in Section 4. We present several numerical results for curve and surface diffusion in Section 5. Finally, conclusions and an outlook to further work are given in Section 6.

Throughou the paper, we shall use standard notation for differential and integral operators, in particular we shall denote partial derivatives of a function u with respect to a variable t by $\frac{\partial u}{\partial t}$ or u_t, and gradients with respect to the spatial variable $\mathbf{x}$ by ∇. Moreover, we shall use standard notation for Lebesgue spaces $L^p(\Omega)$ and Sobolev spaces $W^{k,p}(\Omega)$ and $H^k(\Omega) = W^{k,2}(\Omega)$ (cf. [19] for detailed definitions).

2 Anisotropic Surface Diffusion Flows

In the following we derive the specific form of the chemical potential in anisotropic surface diffusion with curvature-dependent energy. Moreover, we discuss some fundamental properties of surface diffusion flows.

2.1 Surface Energy and Chemical Potential

We start by computing the chemical potential given as the variation of the surface energy $\mathcal{E}$ with respect to the height function u. For this sake we split the energy into

$$\mathcal{E}(u) = \mathcal{E}_1(u) + \mathcal{E}_2(u), \tag{2.1}$$

with $\mathcal{E}_1$ denoting the standard anisotropic term

$$\mathcal{E}_1(u) := \int_\Omega \left(1 + \epsilon \sum_{j=1}^{d+1} n_j^4\right) \, Q \, d\mathbf{x}, \tag{2.2}$$

and with the curvature-dependent term

$$\mathcal{E}_2(u) := \nu \int_\Omega \kappa^2 \, Q \, d\mathbf{x}. \tag{2.3}$$

The derivative of the first term is well established in literature (cf. e.g. [10, 11]), so we just state the corresponding result:

Proposition 2.1. *The first variation of the functional $\mathcal{E}_1$ at $v \in H^1(\Omega)$ in direction $\varphi \in H^1(\Omega)$ is given by*

$$\mathcal{E}_1'(v)\varphi := \int_\Omega \Gamma(\nabla v) \cdot \nabla\varphi \, d\mathbf{x}, \tag{2.4}$$

where Γ is defined by

$$\Gamma(\mathbf{p}) = \nabla_{\mathbf{p}} \left[\sqrt{1 + |\mathbf{p}|^2} + \sum_{j=1}^{d} \frac{p_j^4}{\sqrt{1 + |\mathbf{p}|^2}^3} + \frac{1}{\sqrt{1 + |\mathbf{p}|^2}^3} \right], \tag{2.5}$$

for $\mathbf{p} \in \mathbb{R}^d$.

One can easily show that the surface energy part $\mathcal{E}_1$ is non-convex for $\epsilon > 1/3$ and therefore the corresponding surface diffusion flow would be ill-posed for $\nu = 0$. In the one-dimensional case, we plot the surface tension $1 + \epsilon \sum_{j=1}^{d+1} n_j^4$ as function of u_x for different values of ϵ to illustrate this behaviour.

In order to compute the derivative of the second term, we start with the variation of the curvature term.

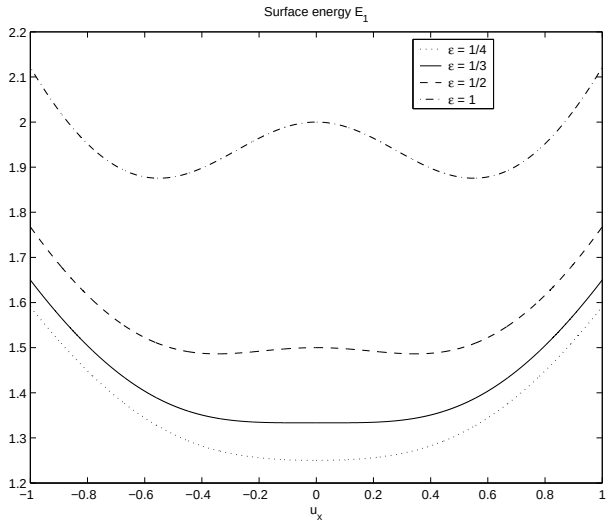

Figure 1: Plot of the surface energy density $1+\epsilon(n_1^4+n_2^4)$ for different values of ϵ.

Lemma 2.2. *Let $v \in H^2(\Omega)$ and define*

$$\kappa(v) := \operatorname{div}\left(\frac{\nabla v}{\sqrt{1+|\nabla v|^2}}\right) \quad \in L^2(\Omega).$$

Then the first variation of κ at v in direction $\varphi \in H^2(\Omega)$ is given by

$$\kappa'(v)\varphi = \operatorname{div}\left(\frac{\mathbf{P}(v)\nabla\varphi}{\sqrt{1+|\nabla v|^2}}\right), \qquad \mathbf{P}(v) = \mathbf{I} - \frac{\nabla v \otimes \nabla v}{1+|\nabla v|^2}. \tag{2.6}$$

Proof. Since the divergence operator is linear and continuous on the function spaces we use, it suffices to compute the derivative of the term $\mathbf{n}(v) = \nabla v/\sqrt{1+|\nabla v|^2}$, which is given by

$$\mathbf{n}'(v)\varphi = \frac{\nabla\varphi}{\sqrt{1+|\nabla v|^2}} - \frac{(\nabla\varphi\cdot\nabla v)\nabla v}{\sqrt{1+|\nabla v|^2}^3},$$

and introducing the matrix $\mathbf{P}(v)$ yields (2.6) □

The above result on the derivative of the mean curvature allows to compute the first variation of $\mathcal{E}_2$:

Proposition 2.3. *Let $u \in H^2(\Omega) \cap W^{1,\infty}(\Omega)$ and $\kappa(u) \in H^1(\Omega)$. Then the derivative of the functional $\mathcal{E}_2$ at u in direction $\varphi \in H^2(\Omega)$ is given by*

$$\mathcal{E}_2'(u)\varphi = \nu \int_\Omega \left(-2\frac{\mathbf{P}(u)\nabla(\kappa Q)}{Q} \cdot \nabla\varphi + \kappa^2 \ \frac{\nabla u \cdot \nabla\varphi}{Q} \right) \ d\mathbf{x}. \tag{2.7}$$

Proof. A standard computation yields

$$\mathcal{E}_2'(u)\varphi = \nu \int_\Omega \left(2\kappa \ Q \ (\kappa'(u)\varphi) + \kappa^2 \ \frac{\nabla u \cdot \nabla\varphi}{Q} \right) \ d\mathbf{x}.$$

By inserting (2.6) and using Gauss' Theorem we deduce (2.7). □

2.2 Basic Properties of Surface Diffusion

In the following we review some basic properties of solutions of the surface diffusion flow. A first natural property of surface diffusion flows is volume conservation, i.e., in absence of a deposition flux, the volume

$$V(t) := \int_\Omega u(\mathbf{x}, t) \ d\mathbf{x} \tag{2.8}$$

is constant. In presence of deposition, the volume change is proportional to the deposited amount of material. This property can easily be verified from the diffusion form (1.8) by multiplying with the constant function $\varphi \equiv 1$ and integrating over Ω, which implies due to Gauss' theorem

$$\frac{dV}{dt}(t) = \int_\Omega u_t(\mathbf{x}, t) \ d\mathbf{x} = -\int_{\partial\Omega} \frac{\nabla\mu}{Q} \cdot \mathbf{n}_{\partial\mathbf{\Omega}} \ da + \int_\Omega f(\mathbf{x}, t) \ d\mathbf{x}.$$

Since the first term on the right-hand side vanishes due to the boundary conditions, we obtain

$$V(t) = V(0) + \int_0^t \int_\Omega f(\mathbf{x}, t) \ d\mathbf{x} \ ds, \tag{2.9}$$

and in particular, the volume remains constant for $f \equiv 0$. Note that the volume conservation is clearly independent on the specific model for the energy functional, but is only caused by the diffusion process. As we shall see below, this property is conserved by the numerical method we use.

A second important property for the surface diffusion flow, which is independent of the specific energy functional and which should be conserved to some extent within a numerical scheme, is the energy decay. To obtain

this kind of estimate we multiply (1.8) by $-\mu$ and (1.6) by u_t and integrate both over Ω. Adding the results yields

$$\int_\Omega \left(\frac{|\mathbf{P}(u)\nabla\mu|^2}{Q} + \mathcal{E}'(u)u_t \right) \, d\mathbf{x} = -\int_\Omega f \, \mu \, d\mathbf{x}.$$

Since $\int_\Omega \mathcal{E}'(u)u_t \, d\mathbf{x} = \frac{d}{dt}\mathcal{E}(u)$, we obtain after integration with respect to time

$$\mathcal{E}(u) + \int_0^t \int_\Omega \frac{|\mathbf{P}(u)\nabla\mu|^2}{Q} \, d\mathbf{x} \, ds = \mathcal{E}(u_0) + \int_0^t \int_\Omega \mathcal{E}'(u) f \, d\mathbf{x} \, ds.$$

Hence, the surface diffusion flow energy exhibits a natural energy decrease except for the external energy source due to deposition.

The energy decay estimate reflects the gradient flow structure of surface diffusion, which is obtained as a gradient flow in the Hilbert space $H^{-1}(\Gamma)$. Following [8], this gradient flow is can be defined as the limit of minimizers $u(t+\tau)$ of

$$\mathcal{E}(u(t+\tau)) + \frac{\tau}{2} \int_\Omega \frac{|\nabla\mu|^2}{Q(t)} \, \Delta x \to \min_{\mu, u(t+\tau)} \tag{2.10}$$

subject to the constraint

$$-\text{div} \left(\frac{\mathbf{P}(u(t))\nabla\mu}{Q(t)} \right) = \frac{u(t+\tau) - u(t)}{\tau}, \tag{2.11}$$

given $u(t)$ and $Q(t) = \sqrt{1 + |\nabla u(t)|^2}$.

3 Discretization of Anisotropic Surface Diffusion

The discretization of surface diffusion with curvature dependent energies faces a similar problem as the discretization of the Willmore flow of surfaces: the derivative of the energy functional involves the term $\nabla(\kappa Q)$ in (2.7). This term reflects the fact that also Gaussian curvature appears in addition to the mean curvature, and hence, a second-order splitting into the natural physical and geometrical variables u, κ, and μ does not suffice.

Following the approach for Willmore flow in [12], we introduce a new variable κQ, which represents a curvature concentration. Hence, we will discretize the surface diffusion flow using the variables

$$(u, v, w) := (u, \kappa Q, -\rho\mu) \tag{3.1}$$

in the following, where $\rho \in \mathbb{R}^+$ is a scaling factor (that will correspond to the inverse of the time step below).

3.1 Time Discretization

The starting point of our approach to the time discretization is the local optimization problem (2.10), (2.11). We introduce the new variable v and rewrite the energy as

$$\hat{\mathcal{E}}(u,v) = \int_\Omega \left(Q + \gamma_0(\nabla u) + \nu \frac{v^2}{Q} \right) \, d\mathbf{x} \tag{3.2}$$

with

$$\gamma_0(\nabla u) = \epsilon \left(\frac{u_x^4}{Q^3} + \frac{u_y^4}{Q^3} + \frac{1}{Q^3} \right), \qquad Q = \sqrt{1 + |\nabla u|^2}. \tag{3.3}$$

Hence, the local optimization problem can be rewritten as

$$\hat{\mathcal{E}}(u,v) + \frac{\tau\rho^2}{2} \int_\Omega \frac{|\mathbf{P}(u(t))\nabla w|^2}{Q(t)} \, d\mathbf{x} \to \min_{u,v,w}, \tag{3.4}$$

subject to the constraints

$$\int_\Omega \left(\frac{\nabla u \cdot \nabla \varphi}{Q} + \frac{v\varphi}{Q} \right) \, d\mathbf{x} = 0, \qquad \forall\ \varphi \in H^1(\Omega) \tag{3.5}$$

and

$$\int_\Omega \left(\frac{(\mathbf{P}(u(t))\nabla w) \cdot \nabla \psi}{Q(t)} + \frac{\rho}{\tau}(u - u(t))\psi \right) \, d\mathbf{x} = 0, \qquad \forall\ \psi \in H^1(\Omega). \tag{3.6}$$

This variational problem already exhibits a certain time discretization and a linearization of the constraint, but still involves the minimization of strongly nonlinear functionals, which we shall approximate further in the following. For the time discretization we use the decomposition $0 = t_0 < t_1 < \ldots < t_N = S$, with time step $\tau_k := t_k - t_{k-1}$ and $\rho_k := \frac{1}{\tau_k}$. We shall denote the solution (u, v, w) at time step t_k by (u^k, v^k, w^k), and define the solution in between via the interpolation

$$u(.,t) = u(.,t_k)\frac{t - t_{k-1}}{\tau_k} + u(.,t_{k-1})\frac{t_k - t}{\tau_k}.$$

In order to obtain a convex quadratic optimization problem instead of (3.4) we use a quadratic expansion of the convex terms and a linear expansion in the potentially non-convex terms, which yields

$$\begin{aligned} \hat{\mathcal{E}}(u^k, v^k) \;\approx\; & \int_\Omega \left(\frac{|\nabla u^k|^2 + |\nabla u^{k-1}|^2}{2Q^{k-1}} + \gamma_0(\nabla u^{k-1}) \right) \, d\mathbf{x} \\ & + \int_\Omega \left(\Gamma_0(\nabla u^{k-1})\nabla(u^{k-1} - u^k) + \nu \frac{(v^k)^2}{Q^{k-1}} \right) \, d\mathbf{x}, \end{aligned}$$

where $\Gamma_0(p) = \nabla_p \gamma_0(p)$. Moreover, we use a lagged diffusivity approximation in the definition of the curvature concentration, i.e., we use Q^{k-1} in the denominators of (3.6). Eliminating the constant terms we can state the semi-discrete optimization problem as the minimization of

$$J^k(u^k, v^k, w^k) = \int_\Omega \left(\frac{|\nabla u^k|^2}{2Q^{k-1}} + \Gamma_0(\nabla u^{k-1}) \cdot \nabla u^{k-1} + \nu \frac{(v^k)^2}{Q^{k-1}} + \rho_k \frac{|\mathbf{P}^{k-1} \nabla w^k|^2}{2Q^{k-1}} \right) d\mathbf{x}$$

subject to the constraints

$$\begin{aligned} \int_\Omega \left(\frac{\nabla u^k \cdot \nabla \varphi}{Q^{k-1}} + \frac{v^k \varphi}{Q^{k-1}} \right) d\mathbf{x} &= 0, \quad \forall\ \varphi \in H^1(\Omega) \\ \int_\Omega \left(\frac{(\mathbf{P}^{k-1} \nabla w^k) \cdot \nabla \psi}{Q^{k-1}} + (u^k - u^{k-1}) \psi \right) d\mathbf{x} &= 0, \quad \forall\ \psi \in H^1(\Omega), \end{aligned}$$

with $\mathbf{P}^{k-1} := \mathbf{P}(u^{k-1})$.

Using additional Lagrangian variables $p^k \in H^1(\Omega)$ and $q^k \in H^1(\Omega)$, we can derive a linear system characterizing the minimizer of this constrained optimization problems. For this sake we again denote the L^2 scalar product by $\langle ., . \rangle$, and define the bilinear forms

$$\mathcal{A}^k(\varphi, \psi) := \int_\Omega \frac{\nabla \varphi \cdot \nabla \psi}{Q^{k-1}}\, d\mathbf{x} \tag{3.7}$$

$$\mathcal{B}^k(\varphi, \psi) := \int_\Omega \frac{(\mathbf{P}^{k-1} \nabla \varphi) \cdot \nabla \psi}{Q^{k-1}}\, d\mathbf{x} \tag{3.8}$$

$$\mathcal{C}^k(\varphi, \psi) := \int_\Omega \frac{\varphi \psi}{Q^{k-1}}\, d\mathbf{x} \tag{3.9}$$

and the right-hand sides

$$(f^k, \psi) := \int_\Omega \Gamma_0(\nabla u^{k-1}) \cdot \nabla \psi\, d\mathbf{x} \tag{3.10}$$

$$(g^k, \psi) := \int_\Omega u^{k-1} \psi\, d\mathbf{x}. \tag{3.11}$$

The semi-discrete problem is then given by computing the weak solution $(u^k, v^k, w^k, p^k, q^k) \in H^1(\Omega)^5$ of the variational equations

$$\begin{aligned} \mathcal{A}^k(u^k, \varphi_1) + \mathcal{A}^k(p^k, \varphi_1) + \langle q^k, \varphi_1 \rangle &= (f^k, \varphi_1) \\ 2\nu \mathcal{C}^k(v^k, \varphi_2) + \mathcal{C}^k(p^k, \varphi_2) &= 0 \\ \rho_k \mathcal{B}^k(w^k, \varphi_3) + \mathcal{B}^k(q^k, \varphi_3) &= 0 \\ \mathcal{A}^k(u^k, \varphi_4) + \mathcal{C}^k(v^k, \varphi_4) &= 0 \\ \mathcal{B}^k(w^k, \varphi_5) + \langle u^k, \varphi_5 \rangle &= (g^k, \varphi_5), \end{aligned} \tag{3.12}$$

for all test function $\varphi_j \in H^1(\Omega)$, $j = 1, \ldots, 5$.

A closer look at this variational problem shows that the Lagrangian variables can be eliminated, because the second equation implies $p^k = -2\nu v^k$ and the third one yields $\nabla q^k = -\rho_k \nabla w^k$. Moreover, since (3.12) is independent of the mean value of q^k, we may choose it such that $q^k = -\rho_k w^k$. Consequently, we arrive at the smaller, but nonsymmetric problem

$$\begin{aligned} \mathcal{A}^k(u^k,\varphi) - 2\nu\mathcal{A}^k(v^k,\varphi) - \rho_k\langle w^k,\varphi\rangle &= (f^k,\varphi), && \forall\ \varphi \in H^1(\Omega) \\ \mathcal{A}^k(u^k,\psi) + \mathcal{C}^k(v^k,\psi) &= 0, && \forall\ \psi \in H^1(\Omega) \\ \mathcal{B}^k(w^k,\eta) + \langle u^k,\eta\rangle &= (g^k,\eta), && \forall\ \eta \in H^1(\Omega). \end{aligned} \tag{3.13}$$

However, this system can easily be made symmetric with minor modifications, e.g., by taking multiples of some lines and changing the order of equations and variables to (v^k, w^k, u^k), we obtain

$$\begin{aligned} \mathcal{C}^k(v^k,\psi) + \mathcal{A}^k(u^k,\psi) &= 0, && \forall\ \psi \in H^1(\Omega) \\ \rho_k\mathcal{B}^k(w^k,\eta) + \rho_k\langle u^k,\eta\rangle &= \rho_k(g^k,\eta), && \forall\ \eta \in H^1(\Omega) \\ \mathcal{A}^k(v^k,\varphi) + \rho_k\langle w^k,\varphi\rangle - \tfrac{1}{2\nu}\mathcal{A}^k(u^k,\varphi) &= -\tfrac{1}{2\nu}(f^k,\varphi), && \forall\ \varphi \in H^1(\Omega). \end{aligned} \tag{3.14}$$

Using standard arguments for symmetric indefinite systems (cf. [5]), one can show that (3.14) is equivalent to the saddle-point problem

$$\inf_{(v,w)} \sup_{u} \mathcal{L}^k(v,w,u),$$

with the Lagrangian

$$\begin{aligned} \mathcal{L}^k(v,w,u) &= \frac{1}{2}\mathcal{C}^k(v,v) + \frac{\rho_k}{2}\mathcal{B}^k(w,w) + \mathcal{A}^k(v,u) + \rho_k\langle w,u\rangle \\ &\quad -\frac{1}{4\nu}\mathcal{A}^k(u,u) - \rho_k(g^k,w) + \frac{1}{2\nu}(f^k,u). \end{aligned}$$

In this form, the curvature concentration v and the chemical potential w play the role of primal, and the height function u plays the role of a dual variable (which obviously could be interchanged).

In order to verify the well-posedness of (3.13), we first transfer the problem into the standard form (cf. [5])

$$\begin{aligned} a((v,w),(\psi,\eta)) + b((\psi,\eta),u) &= (f_1,(\psi,\eta)) && \forall\ (\psi,\eta) \in H^1(\Omega)^2 \\ b((v,w),\varphi) - c(u,\varphi) &= (f_2,\varphi) && \forall\ \varphi \in H^1(\Omega), \end{aligned} \tag{3.15}$$

with the bilinear forms

$$\begin{aligned} a((v,w),(\psi,\eta)) &= \mathcal{C}^k(v,\psi) + \rho_k \mathcal{B}^k(w,\eta) \\ b((v,w),\varphi) &= \mathcal{A}^k(v,\varphi) + \rho_k \langle w,\varphi\rangle \\ c(u,\varphi) &= \frac{1}{2\nu}\mathcal{A}^k(u,\varphi), \end{aligned}$$

and the right-hand sides

$$\begin{aligned} (f_1,(\psi,\eta)) &= \rho_k(g^k,\eta) \\ (f_2,\varphi) &= -\frac{1}{2\nu}(f^k,\varphi). \end{aligned}$$

For the system (3.15), we can use a well-known result for saddle-point problems (cf. [5, p.47]), which we rewrite for the specific setup we use:

Lemma 3.1. *Let a, b, and c, be continuous bilinear forms satisfying the following conditions for positive real constants α_1, α_2, α_3:*

(i) Kernel-ellipticity of a:

$$a((v,w),(v,w)) \geq \alpha_1 \|(v,w)\|^2$$

for all $(v,w) \in H^1(\Omega)^2$ satisfying $b((v,w),.) \equiv 0$.

(ii) Kernel-ellipticity of c:

$$c(u,u) \geq \alpha_2 \|u\|^2$$

for all $u \in H^1(\Omega)$ satisfying $b((.,.),u) \equiv 0$.

(iii) Inf-Sup condition:

$$\inf_{u\in H^1(\Omega)} \sup_{(v,w)\in H^1(\Omega)^2} \frac{b((v,w),u)}{\|u\|(\|v\|+\|w\|)} \geq \alpha_3.$$

Then there exists a unique solution $(u,v,w) \in H^1(\Omega)^3$ of (3.15), and there exists a positive real constant β such that

$$\|u\| + \|v\| + \|w\| \leq \beta\left(\|f_1\| + \|f_2\|\right).$$

We shall now apply this well-posed result to (3.13)

Theorem 3.2. *Let $u^{k-1} \in W^{1,\infty}(\Omega)$. Then there exists a unique weak solution $(u^k,v^k,w^k) \in H^1(\Omega)^3$ of (3.13).*

Proof. Due to Lemma 3.1, it suffices to verify the above conditions (i) -(iii). For the specific form of a we obtain due to the uniform boundedness of Q^{k-1} an estimate of the form

$$a((v,w),(v,w)) \geq m_1 \int_\Omega \left(v^2 + |\nabla w|^2\right)\ d\mathbf{x}.$$

Moreover, if $b((v,w),.) \equiv 0$, we obtain in particular $b((v,w),v) = 0$, which implies an estimate of the form

$$\int_\Omega |\nabla v|^2\ d\mathbf{x} \geq m_2 \int_\Omega w^2\ d\mathbf{x}.$$

Moreover, with $\phi_0 \equiv 1$ we have

$$b((v,w),\phi_0) = \rho_k \int_\Omega w\ dx = 0.$$

Thus, we may combine the above estimates with a Poincaré-type inequality for w, from which we finally arrive at

$$a((v,w),(v,w)) \geq \alpha_1 \int_\Omega \left(v^2 + |\nabla v|^2 + w^2 + |\nabla w|^2\right)\ d\mathbf{x}$$

for some $\alpha_1 > 0$.

Since for $b((.,.),u) = 0$ we obtain in particular $b((u,u),u) = 0$ and hence, $u = 0$, the kernel-ellipticity for the bilinear form c is trivial and follows with $c(u,u) \geq 0$.

In order to verify the inf-sup condition we use the estimate

$$\inf_{u\in H^1(\Omega)} \sup_{(v,w)\in H^1(\Omega)^2} \frac{b((v,w),u)}{\|u\|(\|v\| + \|w\|)} \geq \inf_{u\in H^1(\Omega)} \frac{b((u,u),u)}{2\|u\|^2} \geq \alpha_2 > 0,$$

which is due to the specific form of b and the uniform boundedness of Q^{k-1}. □

We can also incorporate a deposition flux in a straight-forward way by changing g^k to

$$(g^k,\psi) = \int_\Omega (u^{k-1}\psi + \tau_k f\psi)\ d\mathbf{x}.$$

3.2 Finite Element Discretization

For the finite element discretization we shall use piecewise linear elements in the space

$$\mathcal{V}_h := \{\ \varphi \in C^0(\Omega) \cap H^1(\Omega) \mid \varphi|_T \text{ is linear } \}. \tag{3.16}$$

on a regular triangularization $\mathcal{T}_h$ of $\Omega = \bigcup_{T\in\mathcal{T}_h} T$.

The discretization fineness h is given by

$$h = \max_{T\in\mathcal{T}_h} \max_{\mathbf{x}_1,\mathbf{x}_2\in T} |\mathbf{x}_1 - \mathbf{x}_2|.$$

We can directly perform a finite element discretization of (3.13) in $\mathcal{V}_h^3$, which turns out to be equivalent to a finite element discretization of (3.12) in $\mathcal{V}_h^5$ and subsequent elimination of the Lagrange parameters. This yields the following fully discrete scheme:

Scheme 1. Compute an approximation $u_h^0 \in \mathcal{V}_h$ of the initial value u_0.

For $k = 1, \ldots, N$:

- Assemble the right-hand sides

$$(f_h^k, \psi) := \int_\Omega \Gamma_0(\nabla u_h^{k-1}) \cdot \nabla\psi \; d\mathbf{x} \tag{3.17}$$

$$(g_h^k, \psi) := \int_\Omega u_h^{k-1}\psi \; d\mathbf{x}. \tag{3.18}$$

with $Q_h^{k-1} = \sqrt{1 + |\nabla u_h^{k-1}|^2}$ and an approximation f_h of f (using quadrature). Moreover, define the bilinear forms

$$\mathcal{A}_h^k(\varphi,\psi) := \int_\Omega \frac{\nabla\varphi\cdot\nabla\psi}{Q_h^{k-1}} \; d\mathbf{x} \tag{3.19}$$

$$\mathcal{B}_h^k(\varphi,\psi) := \int_\Omega \frac{(\mathbf{P}_h^{k-1}\nabla\varphi)\cdot\nabla\psi}{Q_h^{k-1}} \; d\mathbf{x} \tag{3.20}$$

$$\mathcal{C}_h^k(\varphi,\psi) := \int_\Omega \frac{\varphi\psi}{Q_h^{k-1}} \; d\mathbf{x}, \tag{3.21}$$

with $\mathbf{P}_h^{k-1} = \mathbf{P}(u_h^{k-1})$.

- Compute the discrete solution $(u_h^k, v_h^k, w_h^k) \in \mathcal{V}_h^3$ satisfying

$$\begin{aligned}
\mathcal{A}_h^k(u^k,\varphi) - 2\nu\mathcal{A}_h^k(v^k,\varphi) - \rho_k\langle w^k,\varphi\rangle &= (f_h^k,\varphi), && \forall\ \varphi\in\mathcal{V}_h\\
\mathcal{A}_h^k(u^k,\psi) + \mathcal{C}_h^k(v^k,\psi) &= 0, && \forall\ \psi\in\mathcal{V}_h\\
\mathcal{B}_h^k(w^k,\eta) + \langle u^k,\eta\rangle &= (g_h^k,\eta), && \forall\ \eta\in\mathcal{V}_h
\end{aligned} \tag{3.22}$$

Note that due to the choice of piecewise linear finite elements, ∇u_h^{k-1} and consequently Q_h^{k-1}, $\mathbf{P}_h^{k-1}$ are constant on each triangles, and hence all integrations in the above bilinear forms and the right-hand side f_h^k can be carried out exactly.

As in the semi-discrete setting in Theorem 3.2 we can easily verify the well-posedness of the discrete system. Moreover, we can verify volume conservation for the discrete scheme by using $\eta \equiv 1$. As far as as energy decay is concerned, we obtain from the local variational principle used for constructing the scheme that

$$\hat{\mathcal{E}}(u^k, v^k) + \tau_k \int_\Omega \frac{|\mathbf{P}^{k-1}\nabla\mu^k|^2}{Q^{k-1}}\, d\mathbf{x} \leq \mathcal{E}(u^{k-1}),$$

i.e., the violation of the energy decay is equal to $\hat{\mathcal{E}}(u^k, v^k) - \mathcal{E}(u^k)$, which can be expected to be of first order in time.

4 Solution of the Discretized Problem

Due to the non-symmetric form of the variational problem (3.22), we also obtain a non-symmetric problem for the nodal values $(\mathbf{u}, \mathbf{v}, \mathbf{w}) \in \mathbb{R}^{3N}$ in each step, which is of the form

$$\begin{pmatrix} \mathbf{A} & -2\nu\mathbf{A} & -\rho_k\mathbf{M} \\ \mathbf{A} & \mathbf{C} & \mathbf{0} \\ \mathbf{M} & \mathbf{0} & \mathbf{B} \end{pmatrix} \begin{pmatrix} \mathbf{u} \\ \mathbf{v} \\ \mathbf{w} \end{pmatrix} = \begin{pmatrix} \mathbf{f} \\ \mathbf{0} \\ \mathbf{g} \end{pmatrix}. \tag{4.1}$$

Here, $\mathbf{M}$ is a symmetric mass-matrix, $\mathbf{C}$ is a scaled symmetric mass matrix, and $\mathbf{A}$ and $\mathbf{B}$ are stiffness matrices corresponding to second order elliptic differential operators.

As we have seen above we can transform the system (4.1) to the symmetric one

$$\begin{pmatrix} \mathbf{A} & -2\nu\mathbf{A} & -\rho_k\mathbf{M} \\ -2\nu\mathbf{A} & -2\nu\mathbf{C} & \mathbf{0} \\ -\rho_k\mathbf{M} & \mathbf{0} & -\rho_k\mathbf{B} \end{pmatrix} \begin{pmatrix} \mathbf{u} \\ \mathbf{v} \\ \mathbf{w} \end{pmatrix} = \begin{pmatrix} \mathbf{f} \\ \mathbf{0} \\ -\rho_k\mathbf{g} \end{pmatrix}. \tag{4.2}$$

We can now either interpret u as a primal and (v, w) as dual variables, or vice versa (by suitable reordering of variables and equations). For small system size, in particular in the one-dimensional case, we can solve this linear system by LU- or generalized Cholesky decomposition. For larger systems, we can perform an iterative solution of this symmetric system by

applying standard Krylov-subspace methods like preconditioned GMRES, MINRES, or QMR (cf. [22] for an overview).

Alternatively, we can also obtain the linear system

$$\begin{pmatrix} \mathbf{A} & \mathbf{C} & \mathbf{0} \\ \mathbf{0} & 2\nu\mathbf{A}+\mathbf{C} & \rho_k\mathbf{M} \\ \mathbf{M} & \mathbf{0} & \mathbf{B} \end{pmatrix} \begin{pmatrix} \mathbf{u} \\ \mathbf{v} \\ \mathbf{w} \end{pmatrix} = \begin{pmatrix} \mathbf{0} \\ -\mathbf{f} \\ \mathbf{g} \end{pmatrix}. \tag{4.3}$$

by performing linear manipulations of the first two lines in (4.1). The advantage of (4.3) is that the diagonal blocks are discretizations of elliptic differential operators, while the off-diagonal terms are just mass matrices. Consequently, it seems reasonable to apply a multigrid method as a solver (or as a preconditioner for GMRES) to (4.3), using block Gauss-Seidel smoothers (some care has to be taken of the anisotropic term $\mathbf{B}$). This approach has been used in all the two-dimensional examples presented below and turned out to be a efficient and robust solver.

5 Numerical Results

In the following we present some numerical results for strongly anisotropic surface diffusion flows and some parametric studies in the parameters ϵ and ν, as well as in the coverage (i.e., the volume $V(0)$) and the deposition flux f.

5.1 Curve Diffusion

In the following we present some results for curve diffusion processes, i.e., for Γ being a curve in $\mathbb{R}^2$. For all simulations we used a uniform spatial discretization of $\Omega = (0,1)$ with grid size $h = 10^{-3}$. We start with a the evolution of an interface described by a continuous height function

$$u_0(x) = \begin{cases} \text{constant} & \text{for } x \in [0, 0.25] \cup [0.75, 1] \\ 0.1 + 0.01\cos(4\pi x) & \text{for } x \in (0.25, 0.75) \end{cases}$$

We also use this starting value for the parametric studies below. For the first two simulations we used an anisotropy parameter $\epsilon = 1$ and a curvature coefficient $\nu = 10^{-4}$, in absence of a deposition flux, i.e., $f \equiv 0$.

The obtained evolution (computed with a time step $\tau = 2 * 10^{-6}$) is illustrated by plots of the interfaces obtained at times $t = 4k\tau$, $k = 0, 1, \ldots, 5$, in Figure 2. One observes that faceting, i.e., the formation of flat parts of the interface, occurs already during the early stage of the evolution. The

evolving shape forms several hills and valleys, some of which become unstable and disappears during the later stage. Finally, the interface converges to a shape with three faceted substructures.

The evolution of the surface energy $\mathcal{E}(u(t))$ and the change of the volume $V(t) - V(0)$ are shown in Figure 3. One observes that the energy is decreasing during the evolution as expected and finally becomes constant when the interface has reached an equilibrium shape, which is possibly only a local minimum of the non-convex energy functional. The plot of the volume change confirms the discrete volume conservation, since the maximal error over all timesteps is below the machine precision of 10^{-16}. The same behaviour of the energy and the volume have been observed also in all further simulations presented below.

The second simulation is carried out with the same parameters as the first one, but with the initial height $u_0(x) = 0.1 + 0.005 * \cos(9\pi x)$. In this case, the evolution is faster and we used a time step of $\tau = 4 * 10^{-7}$. We illustrate the obtained evolution by plots of the interface at time $t = 3k\tau$, $k = 0, \ldots, 5$. Again we obtain faceting but in the first example, but the limiting equilibrium shape is a different one, with a higher value of the surface energy and the same orientation of the facets. Hence, this numerical example suggests that the surface diffusion flow can converge to local minima in strongly anisotropic cases, probably to the ones closest to the initial shape.

Our first parametric study varies the anisotropy parameter ϵ for constant $\nu = 10^{-4}$, $f \equiv 0$ and an initial coverage $V(0) = 0.09$. As expected, the surface evolves towards a flat surfaces for $\epsilon < 1/3$, quite similar to the isotropic case $\epsilon = 0$, but of course faster for smaller ϵ. Therefore, we only show the more interesting results for the strong anisotropies $\epsilon = 0.5, 1, 1.5, 2$ in Figure 5. The first two plots show the front Γ at time steps $t = 0, 10^{-5}, \ldots, 2 * 10^{-4}$, and the plots for higher ϵ show the the front Γ at time steps $t = 0, 10^{-6}, \ldots, 2 * 10^{-5}$. One observes that the time scale of the evolution reduces with increasing ϵ, i.e., the evolution towards an equilibrium and the faceting is faster for higher anisotropy. Moreover, the length scale of the evolving and equilibrium structures decreases with increasing anisotropy parameter, which is caused by the changing orientation of facets. From our simulations it seems that the maximal height of the film does not exceed a certain maximal value, but for larger ϵ there occurs a transition from three to five hills and valleys. Hence the facets become steeper as expected, but the maximum height can even decrease compared to smaller values ϵ.

A second parametric study concerns the coefficient ν of the curvature term. We illustrate the results for $\nu = 10^{-m}$, $m = 1, \ldots, 5$, fixing $\epsilon =$

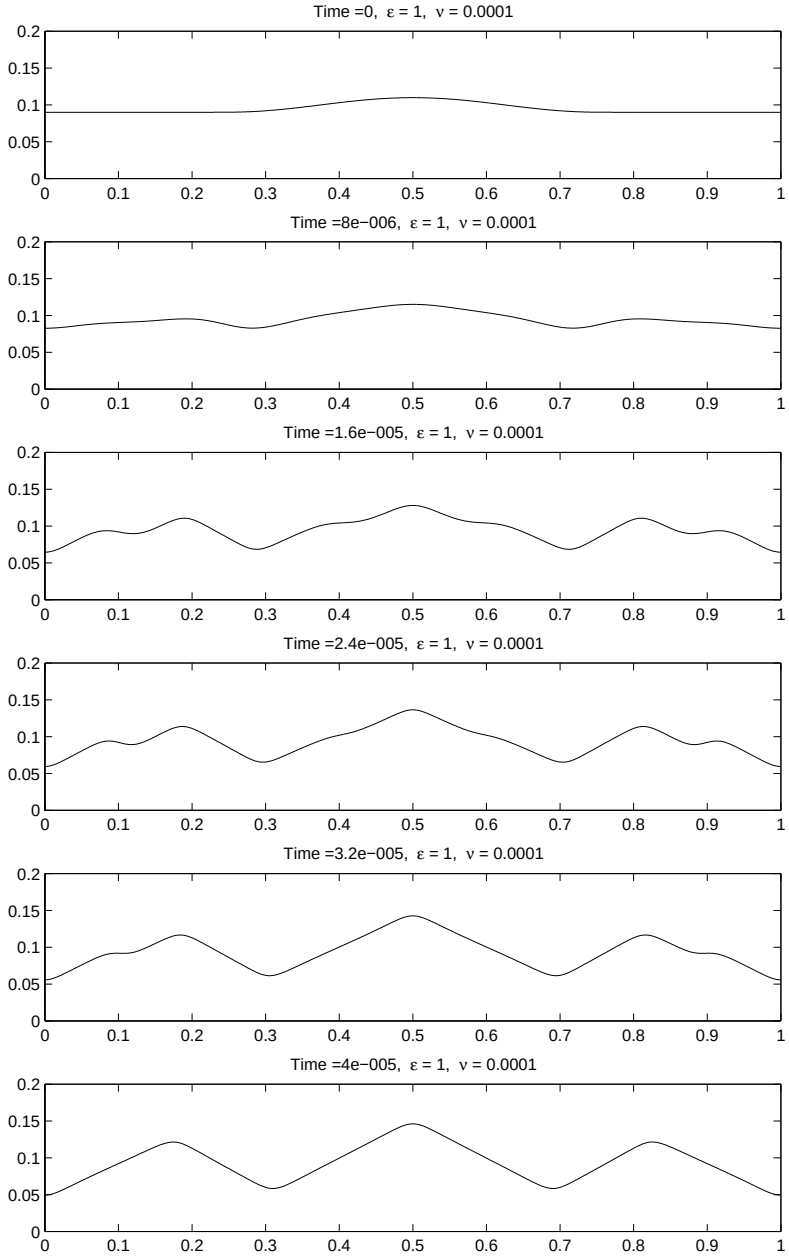

Figure 2: Evolution of the interface for $\epsilon = 1$, $\nu = 10^{-4}$, $f \equiv 0$, for the first initial value.

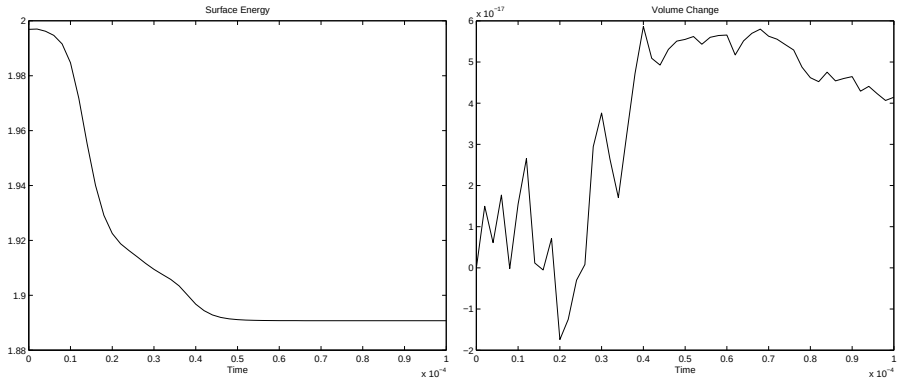

Figure 3: Evolution of the surface energy (left) and the volume (right) for $\epsilon = 1$, $\nu = 10^{-4}$, $f \equiv 0$, for the first initial value.

1, $f \equiv 0$, and $V(0) = 0.09$. In Figure 6 we plot the evolving fronts at time steps $0, 10^{-5}, \ldots, 2 * 10^{-4}$, except for $\nu = 10^{-5}$, where we use the more appropriate time steps $0, 2 * 10^{-6}, \ldots, 4 * 10^{-5}$. One observes that for increasing values of ν, the size of the rounded parts of the surface increases (and consequently, their curvature decreases), while the orientation of the faceted parts remains the same (except for very large values of ν, where the curvature effect becomes global). Moreover, the time and spatial scale are changing with ν.

Figure 7 illustrates the effects of varying the coverage $V(0)$ by plotting the evolving interfaces at times $t = 0, 10^{-5}, \ldots, 2 * 10^{-4}$, for the coverages $V(0) = 0.045, 0.09, 0.18, 0.36, 0.72$, and 1.44. One observes that the shapes are similar for the smaller values of the initial coverage, but for the largest value (where the height becomes larger than the length) there is a transition in the equlibrium shape.

Our final parametric study concerns the deposition flux f. We perform tests with two uniform deposition fluxes, $f \equiv 10^2$ and $f \equiv 10^3$, as well as with a linearly increasing flux $f = 10^3 x$ and a parabolic flux profile $f = 4 * 10^3 x(1-x)$. The resulting interfaces at times $t = 0, 10^{-5}, \ldots, 2 * 10^{-4}$ are plotted in descending order in Figure 8. For the spatially homogeneous deposition fluxes one observes a very similar evolution as in the absence of deposition flux, but with linearly growing height. For the spatially varying deposition flux, we obviously obtain faster growth in areas of higher flux, but still the orientation of facets remains unchanged.

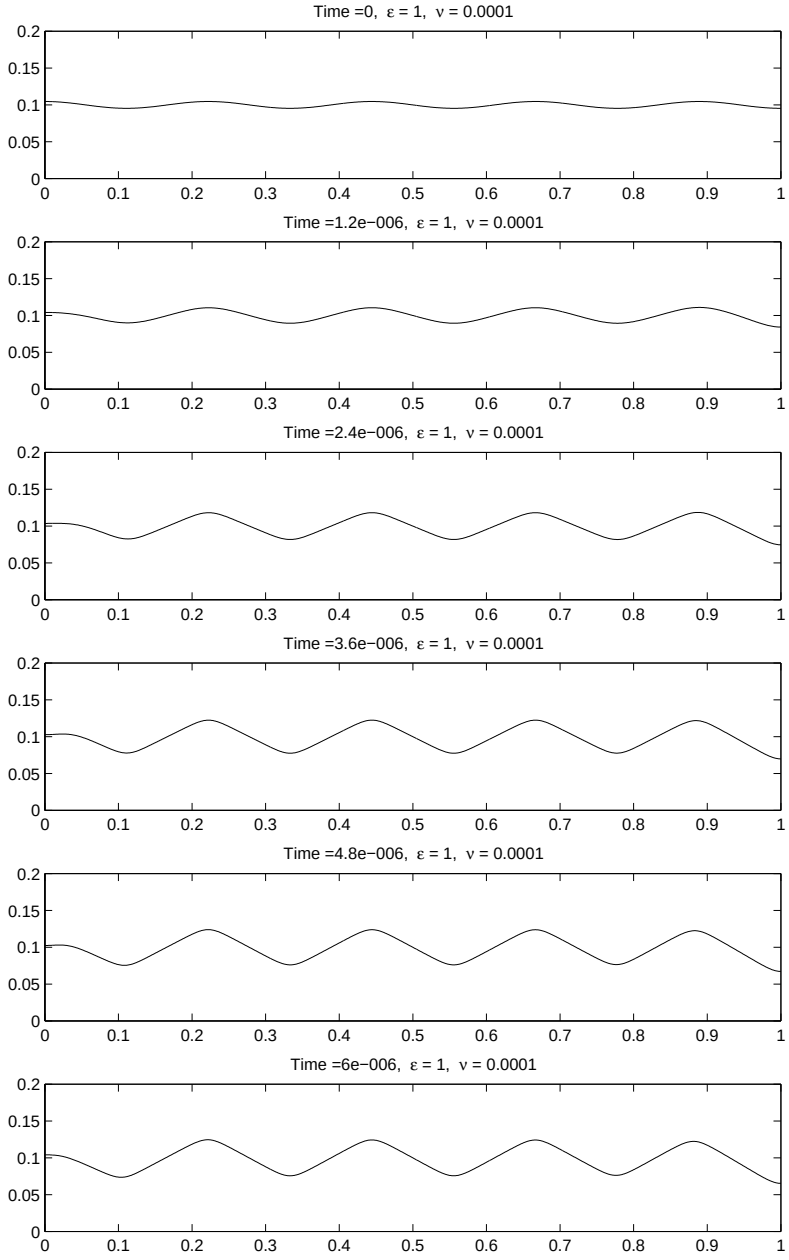

Figure 4: Evolution of the interface for $\epsilon = 1$, $\nu = 10^{-4}$, $f \equiv 0$, for the second initial value.

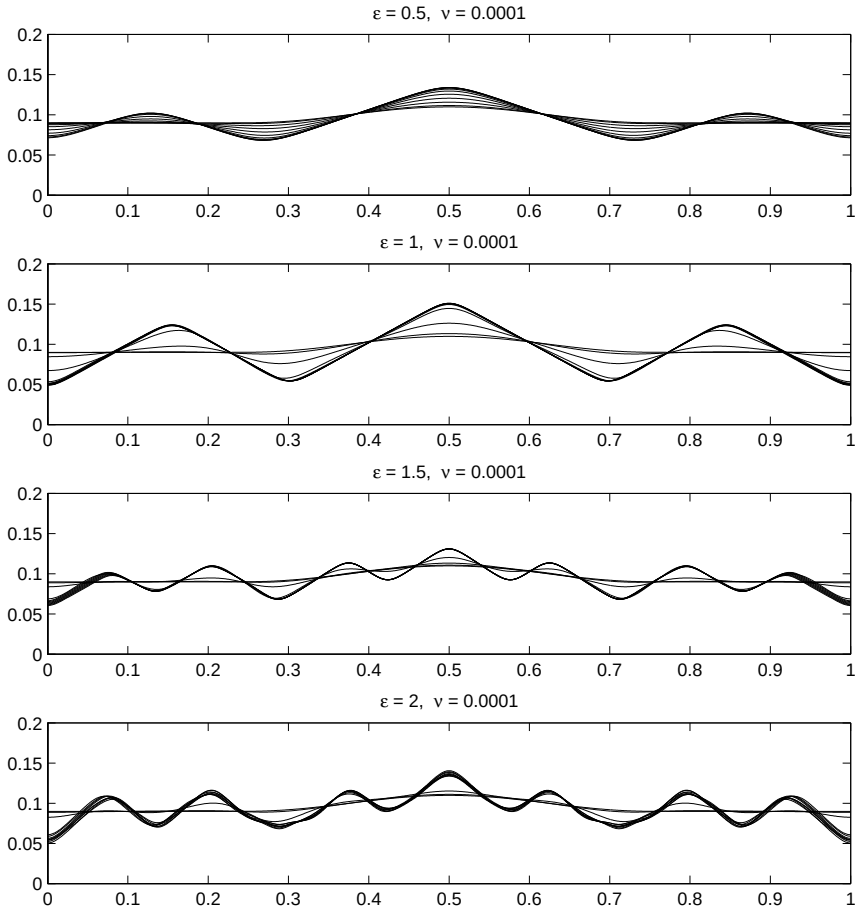

Figure 5: Evolution of the interface for different values of the anisotropy parameter ϵ.

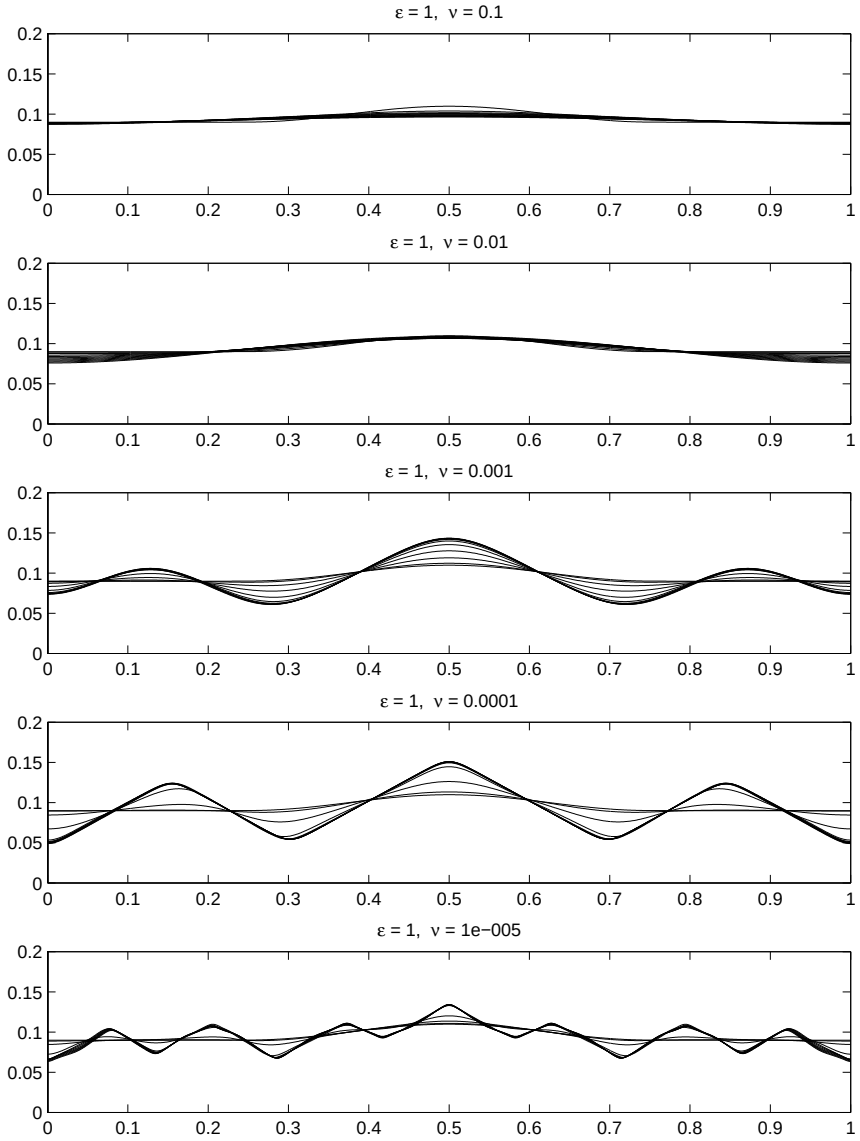

Figure 6: Evolution of the interface for different values of ν.

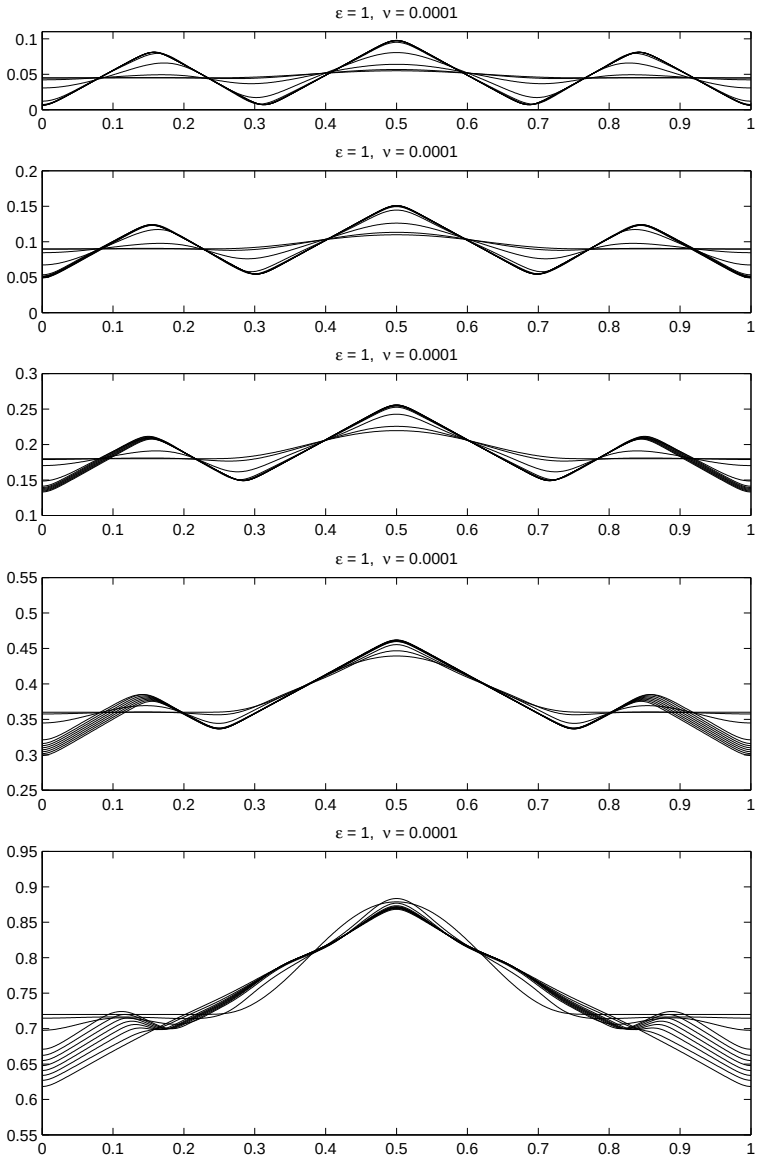

Figure 7: Evolution of the interface for different initial coverages $V(0)$.

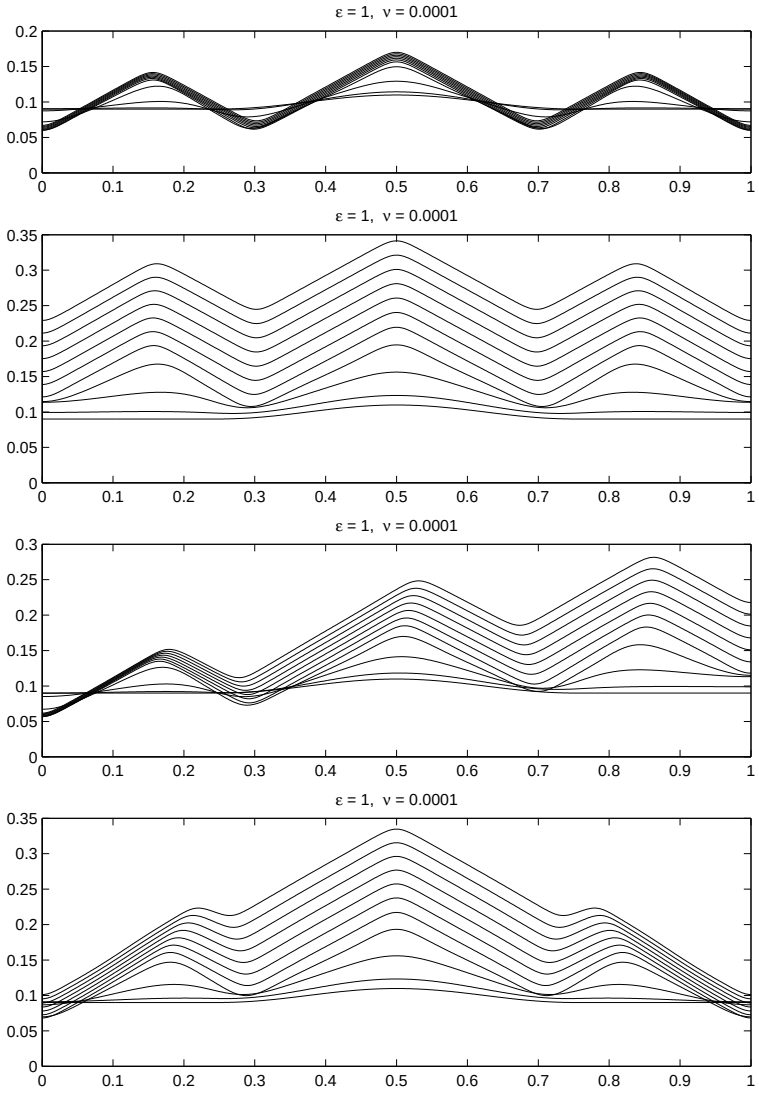

Figure 8: Evolution of the interface for different deposition fluxes f.

5.2 Surface Diffusion

We now present two results for surface diffusion, which are both obtained for $\epsilon = 0$, $\nu = 10^{-3}$, and $f \equiv 0$. The computational domain is given by $\Omega = (-1, 1)^2$, and the discretization is performed on a regular grid of size $h = 10^{-2}$, with a time step $\tau = 10^{-2}$.

In the first example, we use the initial value

$$u_0(x, y) = 0.2 - 0.05 \cos(\pi x) \cos(\pi y).$$

In Figure 9 we plot the resulting surface at times $t = 3k\tau$, $k = 1, \ldots, 5$, and after a larger time at $t = 0.5$ (from top to bottom). One observes that faceting occurs mainly in the early stage of the evolution, and the arising shapes seem to converge to a local energy minimum. The evolution therefore becomes almost stationary in the later stage.

In the second example, we divide the wavelength by two in the initial value, i.e., we use

$$\hat{u}_0(x, y) = 0.2 - 0.05 \cos(2\pi x) \cos(2\pi y).$$

Figure 10 shows plots of the obtained surfaces at the same time steps as for the first example. The behaviour is similar, but the local energy minimizer the evolution converges to is a different one.

We finally mention that parametric studies with respect to ϵ, ν, f, and $V(0)$ lead to similar results as for curve diffusion.

6 Conclusions and Outlook

We have presented numerical methods for surface diffusion arising in systems with anisotropic surface energies involving a curvature dependent term, and discussed some of their properties. The presented numerical results confirmed the applicability of this approach to strongly anisotropic cases, where faceting of the evolving curves or surfaces occurs, while the corners are rounded.

To our knowledge, this paper presents the first simulation of the full surface diffusion model with curvature dependent energy. Due to the practical importance of this problem, the methods and results presented here are also the starting point towards the simulation of several crystal growth phenomena that can be modeled by anisotropic surface diffusion, and the coupling with other physical effects such as elastic relaxation in heteroepitaxial growth (cf. e.g. [18]) having in mind important technological applications such as self-assembled silicon-germanium quantum dots (cf. e.g. [4]).

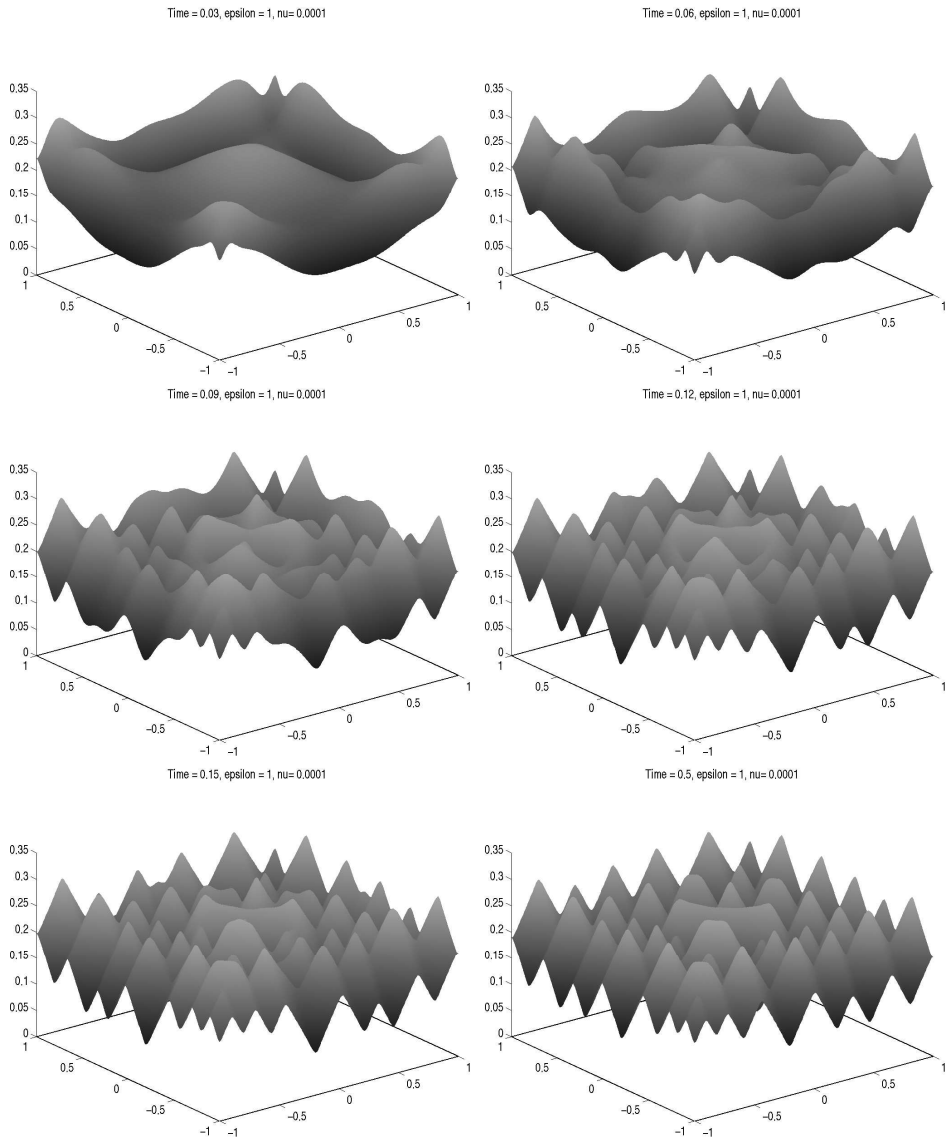

Figure 9: Evolution of the surface for the initial value u_0 .

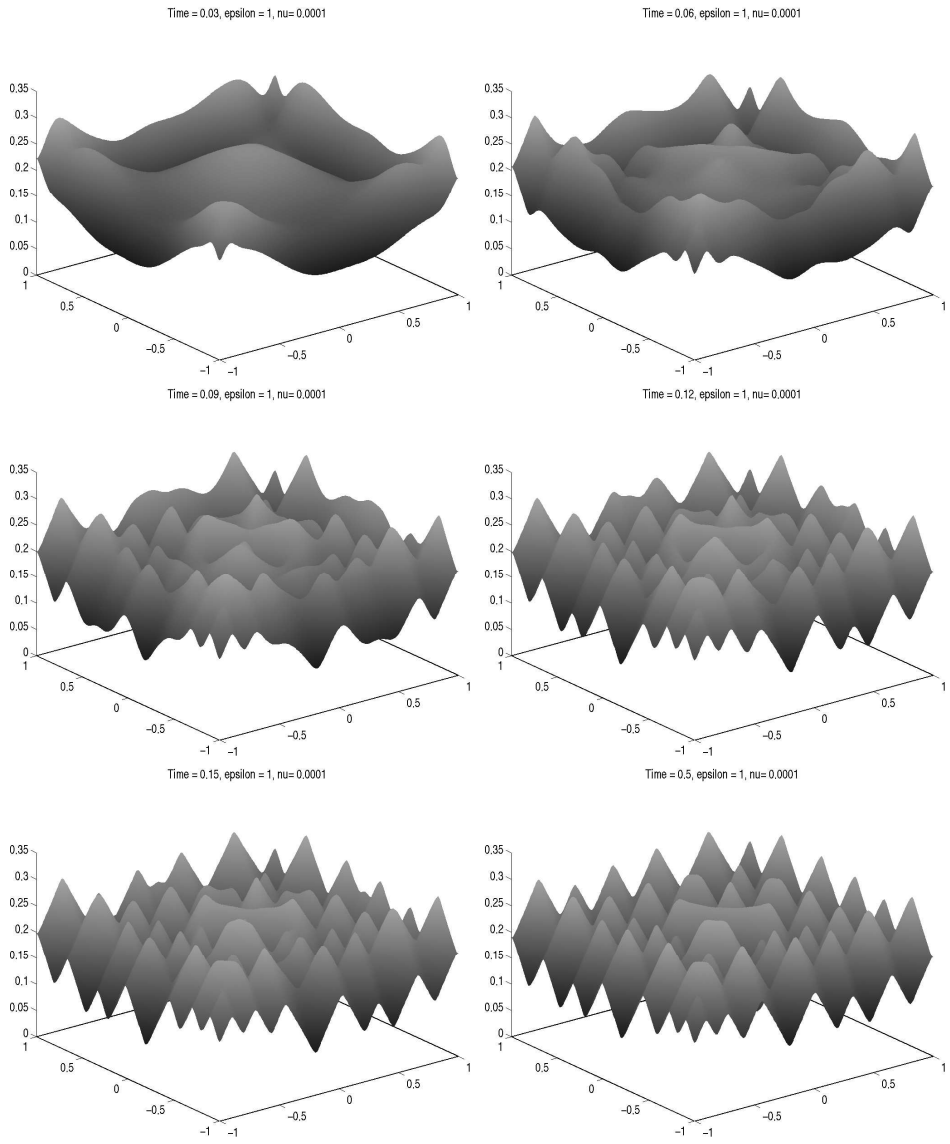

Figure 10: Evolution of the surface for the initial value $\hat{u}_0$.

From a mathematical viewpoint, an important task for future researchis the detailed analysis of the surface diffusion model and the numerical methods, which is rather incomplete in the isotropic case (cf. [3, 13, 20]), and completely open in the anisotropic case with curvature dependence.

Acknowledgements

The author thanks Günther Bauer (University Linz) for initiating his interest in surface diffusion and many stimulating discussions, and Russel Caflisch (UCLA) for further stimulating discussions. Financial support is acknowledged to the NSF through ITR grant ACI-0321917 and to the ONR through grant N00014-02-1-0720.

References

[1] E.Bänsch, P.Morin, R.Nochetto, *Surface diffusion of graphs: Variational formulation, error analysis, and simulation*, Preprint (WIAS Berlin, 2003).

[2] E.Bänsch, P.Morin, R.Nochetto, *Finite element methods for surface diffusion*, Preprint (WIAS Berlin, 2003).

[3] P.Baras, J.Duchon, R.Robert, *Evolution d'une interface par diffusion de surface*, Comm. Partial Diff. Eq. **9** (1984), 313-335.

[4] G.Bauer, A.A.Darhuber, V.Holy, *Self-assembled Germanium-dot multilayers embedded in Silicon*, Crystal Research and Technololgy **34** (1999), 197-209.

[5] F.Brezzi, M.Fortin, *Mixed and Hybrid Finite Element Methods*, (Springer, New York, 1991).

[6] J.W.Cahn, J.E.Taylor, *Surface motion by surface diffusion*, Acta Metall. Mater. **42** (1994), 1045-1063.

[7] W.C.Carter, A.R.Roosen, J.W.Cahn, J.E.Taylor, *Shape evolution by surface diffusion and surface attachment limited kinetics on completely faceted surfaces*, Acta Metall. Mater. **43** (1995), 4309-4323.

[8] W.C.Carter, J.E.Taylor, J.W.Cahn, *Variational methods for microstructural evolution*, JOM: Member J. Minerals Metals Materials Soc. **49** (1997), 30-36.

[9] F.Davi, M.E.Gurtin, *On the motion of a phase interface by surface diffusion*, J. Appl. Math. Phys. **41** (1990), 782-811.

[10] K.Deckelnick, G.Dziuk, *A fully discrete numerical scheme for weighted mean curvature flow*, Numer. Math. **91** (2002), 423-452.

[11] K.Deckelnick, G.Dziuk, C.M. Elliott, *Fully discrete semi-implicit second order splitting for anisotropic surface diffusion of graphs*, Preprint (Isaac Newton Institute, Cambridge, 2003).

[12] M.Droske, M.Rumpf, *A level set formulation for Willmore flow*, Interfaces and Free Boundaries (2004), to appear.

[13] C.M.Elliott, H.Garcke, *Existence results for diffusive surface motion laws*, Adv. Math. Sci. Appl. **7** (1997), 465–488.

[14] A.A.Golovin, S.H.Davis, *Effect of anisotropy on morphological instability in the freezing of a hypercooled melt*, Physica D **116** (1998), 363-391.

[15] A.A.Golovin, S.H.Davis, A.A.Nepomnyashchy, *A model for facetting in a kinetically controlled crystal growth*, Phys. Rev. E **59** (1999), 803-825.

[16] M.E.Gurtin, *Thermomechanics of Evolving Phase-Boundaries in the Plane* (Oxford University Press, Oxford, 1993).

[17] M.E.Gurtin, M.E.Jabbour, *Interface evolution in three dimensions with curvature-dependent energy and surface diffusion: Interface-controlled evolution, phase transitions, epitaxial growth of elastic films*, Arch. Rat. Mech. Anal. **163** (2002), 171-208

[18] F.Jonsdottir, L.B.Freund, *Equilibrium surface roughness of a strained epitaxial film due to surface diffusion induced by interface misfit dislocations*, Mech. Materials **20** (1995), 337-349.

[19] J.L.Lions, E.Magenes, *Non-Homogenous Boundary Value Problems and Applications, Vol. I* (Springer, Berlin, Heidelberg, New York, 1972).

[20] V.Lods, A.Piétrus, J.M.Rakotoson, *Mathematical study of the equation describing the evolution of the surface of a film*, Asymptotic Analysis **33** (2003), 67-91.

[21] W.W.Mullins, *Theory of thermal grooving*, J. Appl. Phys. **28** (1957), 333-339.

[22] Y.Saad, *Iterative Methods for Sparse Linear Systems* (2nd Ed., SIAM, Philadelphia, 2003).

[23] T.V.Savina, A.A.Golovin, S.H.Davis, A.A.Nepomnyashchy, P.W.Voorhees, *On faceting of a growing crystal surface by surface diffusion*, Phys. Rev. E **67** (2003), 1-16.

[24] J.Stewart, N.D.Goldenfeld, *Spinodal decomposition of a crystal surface*, Phys. Rev. A **46** (1992), 6505-6512.

[25] W.Zhang, I.Gladwell, *Evolution of two-dimensional crystal morphologies by surface diffusion with anisotropic surface free energies*, Comp. Mat. Science **27** (2003), 461-470.